Journal of Controlled Release 232 (2016) 42–50

Contents lists available at ScienceDirect

Journal of Controlled Release

journal homepage: www.elsevier.com/locate/jconrel

# Mechanisms allowing protein delivery in nasal mucosa using NPL nanoparticles

B. Bernocchi [a,b,c], R. Carpentier [a,b,c,*], I. Lantier [e,f], C. Ducournau [f,e], I. Dimier-Poisson [f,e], D. Betbeder [a,b,c,d]

[a] Inserm, LIRIC—UMR 995, F-59000 Lille, France
[b] Université de Lille, LIRIC—UMR 995, F-59000 Lille, France
[c] CHRU de Lille, LIRIC—UMR 995, F-59000 Lille, France
[d] University of Artois, 62000 Arras, France
[e] INRA, UMR1282 Infectiologie et Santé Publique, F-37380 Nouzilly, France. Laboratoire d'Expertise en Infection Animale
[f] Université François-Rabelais de Tours, UMR1282 Infectiologie et Santé Publique, F-37000 Tours, France. Immunologie Parasitaire et Vaccinologie, Biothérapies Anti-Infectieuses

ARTICLE INFO

*Article history:*
Received 24 February 2016
Received in revised form 31 March 2016
Accepted 6 April 2016
Available online 11 April 2016

*Keywords:*
Nanoparticle
Intranasal drug delivery
Protein delivery
Transcytosis
Biodistribution
Vaccine

ABSTRACT

The intranasal administration of proteins using nanoparticles is a promising approach for several applications, especially for mucosal vaccines. Delivery of protein within the epithelial barrier is a key point to elicit an immune response and nano-carrier has to show no toxicity. The aim of this work was to elucidate the interactions of cationic porous nanoparticles loaded with protein delivery for antigen delivery in the nose. We investigated the loading, the cellular delivery and the epithelial transcytosis of proteins associated to these nanoparticles containing an anionic lipid in their core (NPL). NPL were highly endocytosed by airway epithelial cells and significantly improved the protein delivery into the cell. *In vitro* transcytosis studies showed that NPL did not modify the *in vitro* epithelial permeability suggesting no toxicity of these carriers. Moreover protein and NPL did not translocate the epithelial barrier. *In vivo* studies demonstrated that NPL prolonged the nasal residence time of the protein and no NPL were found beyond the epithelial barrier *in vivo*, precluding a negative side effect. All together these results establish the NPL as a bio-eliminable and optimal vaccine carrier.



## 1. Introduction

In recent years, nanoparticles have been increasingly studied for use in vaccine applications [1–3] owing to their potential adjuvant effect and ability to mimic viruses, characteristics related to their size, geometry and physical properties [4]. Furthermore, researchers have repeatedly reported that the use of particulate antigens is more successful than soluble ones in activating immune cells and affording longer term protection [5–7].

The mucosal route of administration is promising in order to trigger an effective immune response and protection against pathogens [8], and offers the possibility of needle-free vaccinations [9]. Notably, the nasal route is a convenient mucosal site for vaccine delivery since, besides being the natural route of infection of many pathogens, it is also non-invasive [10,11].

The translocation of nanoparticles has been extensively investigated at the blood-brain and the intestinal barriers [12–16]. However, little is known about transcytosis of nanoparticles in the airway mucosa. Scarce *in vitro* evaluations have been conducted in models of the airway epithelial barrier to improve understanding of the permeation mechanisms governing drug and nanocarrier passage through the epithelium [17–19], but fewer *in vivo* studies have been published [20–23].

Paracellular transport is also considered as a potential pathway to overcome epithelial barriers [24] and to deliver drugs to immune cells found beneath the epithelium. The tight junction (TJ) opening can improve the drug permeation, although it could also be the result of a toxic effect [25]. Several *in vitro* models have been used to explore the interaction of xenobiotics with the airway epithelium. Human nasal septum epithelial cells RPMI2650 ATCC® CCL-30™ were used however these cells pile and fail to reach a complete confluence [26,27]. The 16HBE14o-human bronchial epithelial cell line are useful in the study of paracellular drug transport, since they form a pseudo-stratified monolayer and express TJ proteins [28–30] and have been established as a model system to investigate drug transport across the airway epithelium [31].

Porous nanoparticles [32] have recently been studied as vaccine delivery vectors [33]. It is possible to load these nanoparticles with proteins in order to deliver them into cells *via* endocytosis [34] and their use as nasal delivery systems for antigens has been shown to protect mice from acute and chronic infection against *Toxoplasma gondii* [33]. However, the mechanisms by which these nanoparticles deliver antigens within the airway mucosa and their ability to cross epithelial barriers have yet to be fully clarified.

* Corresponding author at: Inserm, LIRIC—UMR 995, F-59000 Lille, France.
*E-mail address:* rodolphe.carpentier@univ-lille2.fr (R. Carpentier).

http://dx.doi.org/10.1016/j.jconrel.2016.04.014

In this work we aimed to better understand the interactions of these nanoparticles with the airway epithelial cells, their ability to cross this barrier, and to analyze the impact of the lipids within these nanoparticles on the delivery and the transcytosis of antigens in epithelial cells. *In vivo* studies were performed to track the antigen delivery in airway mucosa and its biodistribution after nasal administration. Toxicity issues are discussed.

## 2. Materials and methods

### 2.1. $NP^+$ and NPL preparation

Polysaccharidic nanoparticles ($NP^+$) and polysaccharidic lipidated nanoparticles (NPL) were prepared from maltodextrin (Roquette, France) as described previously by Paillard et al. [32]. Briefly, maltodextrin was dissolved in water by magnetic stirring at room temperature. A mixture of epichlorohydrin and glycidyltrimethylammonium chloride (GTMA, a cationic ligand; both from Sigma-Aldrich, France) in basic medium was added to the cationic polysaccharide leading to the formation of a gel. The gel was then neutralized with acetic acid and crushed with a high pressure homogenizer (Emulsiflex C3, Avestin, Germany). The nanoparticles ($NP^+$) thus obtained were purified by tangential flow ultra-filtration (Centramate Minim II PALL, France) using a 1000 kDa membrane (PALL, France) to remove oligosaccharides, low-molecular weight reagents and salts. Purified $NP^+$ were freeze dried. Lyophilized $NP^+$ were resuspended in a 70% (w/w) aqueous solution of an anionic lipid (DPPG: 1,2-dipalmitoyl-*sn*-glycero-3-phosphatidylglycerol from Lipoid, Germany) which was incorporated by the nanoparticles, thus obtaining NPL.

### 2.2. Labeling of the polysaccharide part of NPL

$NP^+$ were covalently labeled with fluorescein isothiocyanate (FITC, Sigma-Aldrich, France) according to the following protocol: FITC was added to $NP^+$ ($NP^+$/FITC mass ratio of 10), solubilized in 0.1 M bicarbonate buffer (pH 9.5), and the solution was mixed for 6 h in the dark at room temperature. Afterwards the $NP^+$-FITC were purified by tangential flow filtration and lyophilized. The $NP^+$-FITC were then lipidated, as described above, in order to obtain NPL-FITC.

### 2.3. Labeling of the lipid part of NPL

Labeling of the phospholipids encapsulated in the NPL with DiD (1.1′-Dioctadecyl-3,3,3′,3′-Tetramethylindodicarbocyanine Perchlorate, ThermoFisher Scientific, France) was performed by mixing DiD (1 mg/ml in ethanol) for 30 min at room temperature with NPL with a final concentration of 0.7% (w/w of DPPG) obtaining NPL-DiD. After organic solvent evaporation the formulations were kept in the dark at 4 °C before use, while DiD loading was confirmed by gel permeation studies on a PD-10 Sephadex G25 desalting column (Sigma-Aldrich, France).

### 2.4. Protein labeling and loading into nanoparticles

The ovalbumin (OVA, Sigma-Aldrich, France) was labeled with FITC (Fluorescein-5-isothiocyanate, ThermoFisher Scientific), TRITC (tetramethylrhodamine-5-isothiocyanate, ThermoFisher Scientific, France) or CF750® Succinimidyl ester (Sigma-Aldrich, France) following the same protocol used for the $NP^+$ labeling. The labeled protein was purified by gel filtration on a PD-10 Sephadex column, as above. The concentration of the labeled protein was then evaluated using the Micro BCA Protein Assay Kit (ThermoFisher Scientific, France) following the supplier's instructions. Labeled OVA (1 mg/ml) was post-loaded into pre-made sterile NPL (5 mg/ml) by mixing increasing amounts of OVA obtaining 1:0.5, 1:3 and 1:5 (w/w) OVA:NPL formulations.

### 2.5. Characterization of the NPL

The characterization of the size and zeta potential of the NPL were performed with a Zetasizer nanoZS (Malvern Instruments, France). For the size analysis, NPL (5 mg/ml) were directly measured. For the zeta potential analysis, 12 μl of NPL (5 mg/ml) were diluted to a final volume of 750 μl using distilled water and loaded into a disposable, folded capillary cell.

### 2.6. Characterization of OVA:NPL formulations

The size and the zeta potential of the OVA:NPL formulations were determined as described above. The analysis of the protein association to the NPL was performed by native polyacrylamide gel electrophoresis (PAGE), supplementing the formulations with electrophoresis buffer (Tris-HCL 125 Mm (pH 6.8), 10% glycerol, 0.06% bromophenol blue) and running the samples on a 10% acrylamide-bisacrylamide gel. A silver nitrate staining was subsequently performed to detect the unbound proteins and thus evaluate the amount of associated proteins.

### 2.7. NPL endocytosis and in vitro protein delivery

The 16HBE14o-(16HBE) human bronchial epithelial cell line obtained from Dr. Gruenert D. C. (Colchester, Vermont, USA), was maintained in Dulbecco's Modified Eagle Medium (DMEM, ThermoFisher Scientific, France) supplemented with 10% heat-inactivated Fetal Calf Serum (FCS, ThermoFisher Scientific, France), 100 U/ml Penicillin, 100 mg/ml streptomycin and 1% L-glutamine at 37 °C in a humidified 5% $CO_2$ atmosphere. The cells were plated at a density of $7.5 \times 10^5$ cells/well in 6-well plates and used once they reached the confluence, after two days. The cells were treated for different times (0, 0.5, 1, 3, and 24 h) with NPL-FITC, NPL-DiD or with free OVA-FITC or OVA-FITC formulated in NPL. The cells were then analyzed with a BD Accuri™ C6 CFlow Sampler flow cytometer (BD Bioscience, USA).

### 2.8. In vitro transcytosis of NPL and ovalbumin across the airway epithelium

The *in vitro* transcytosis of NPL was investigated in a Transwell® model of the respiratory epithelial barrier. The 16HBE cells were seeded on Transwell® filters (3 μm porosity Transwell® filters, BD Bioscience, France) at a density of $1 \times 10^5$ cells/Transwell® (0.9 $cm^2$). The confluence was checked by transepithelial electrical resistance (TEER) measurement with an epithelial Voltohmmeter (EVOM2, World Precision Instrument, USA) equipped with an STX2 electrode. The cells were pre-incubated for 30 min with Hank's Balanced Salt Solution (HBSS, Life Technologies, France) at 37 °C before measuring the permeability. A low molecular weight chitosan (Sigma-Aldrich, France) solution in HBSS at pH 6.5 (0.05% w/v) was used as positive control for the TJ opening and a 50 μg/ml solution of lucifer yellow (Sigma-Aldrich, France) as control for the paracellular and transcellular transport [35,36].

The cell monolayers were treated with 25 μg of NPL-FITC, NPL-DiD or with OVA-TRITC:NPL formulation, using HBSS as donor and acceptor medium. The TEER was checked after 30 min and every hour for 3 h moving the Transwell® in a plate with fresh acceptor medium before each measurement. The samples from the apical side and basolateral side were collected separately and the fluorescence was measured with a Fluoroskan Ascent™ Microplate Fluorometer (Thermo Scientific, France).

### 2.9. Mice

Six-to-eight week-old Swiss OF1 mice were purchased from CER Janvier (France) and maintained under conventional conditions. Experiments were carried out in accordance with the guideline for

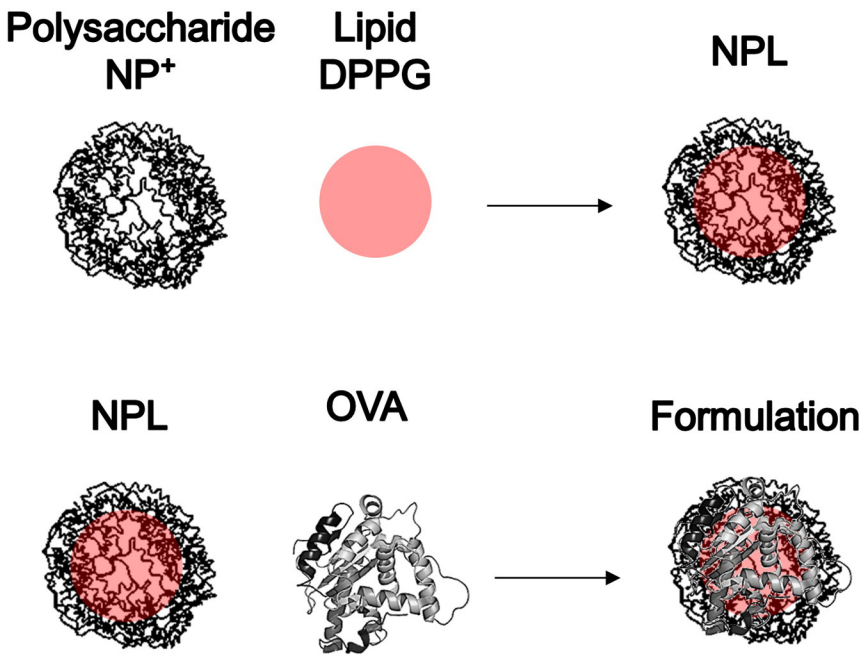


**Fig. 1.** Representation of NPL and ovalbumin (OVA) formulation. Premade polysaccharidic positive $NP^+$ are post-loaded with an anionic lipid to obtain NPL. The antigenic protein is postloaded in NPL to prepare the formulation.

**Table 1**
Characterization of the formulations OVA:NPL. Size (Z-average), PDI (polydispersity index) and Zeta potential are measured in triplicate with a Zetasizer NanoZS.

| | Z-average (nm) | PDI | Zeta-potential (mV) |
|---|---|---|---|
| $NP^+$ | 70.39 | 0.233 | +45.9 ± 6.86 |
| NPL | 76.07 | 0.211 | +44.2 ± 10.15 |
| OVA | 1.976 | 0.477 | −7.77 ± 5.60 |
| OVA:NPL 1:0.5 w/w | 2782.67 | 1 | +25.17 ± 6.937 |
| OVA:NPL 1:3 w/w | 76.71 | 0.261 | +33.27 ± 9.173 |
| OVA:NPL 1:5 w/w | 62.39 | 0.236 | +33.47 ± 8.417 |

animal experimentation (EU Directive 2010/63/EU) and the protocol was approved by the local ethics committee at Tours University (CEEA VdL).

To eliminate the background fluorescence caused by the grain-based diet, the animals were fed with the AIN-93M purified and dedicated diet for fluorescence optical imaging (TestDiet, United Kingdom) 7 days before instillation, and throughout the *in vivo* biodistribution study. To reduce background signal and light absorbance due to their fur, the animals were treated with depilatory cream one day before instillation and imaging process.

### *2.10. In vivo biodistribution studies of OVA alone or loaded in NPL after nasal administration*

Three groups of non-anesthetized mice (3 mice/group) were designated as follows: control group (PBS), CF750® labeled ovalbumin (OVA-CF750®), formulation OVA-CF750®:NPL ratio 1:3 (w/w). Mice were administered with 10 μg of protein by nasal instillation, 5 μl in each nostril. The three groups of mice were maintained in separate boxes with water and diet *ad libitum*.

Longitudinal studies in individual animals were performed using the *In Vivo* Imaging System IVIS® Spectrum (PerkinElmer, Waltman, USA). Mice groups were successively imaged at 0.5, 1, 1.5, 2, 2.5, 3, 6, 24, 48 h following instillation, and one of the control mice was also imaged with each group at each time point. Acquisitions and analyses of images thus obtained were performed with the PerkinElmer Living Image software (version 4.2).

### *2.11. In vivo biodistribution studies of OVA and OVA:NPL in nostrils*

Non-anesthetized mice were given 20 μl nasal instillations of solutions containing 8.3 μg of OVA-TRITC or the same amount of OVA-TRITC loaded in NPL-FITC at the ratio 1:3 (w/w). As a negative control,

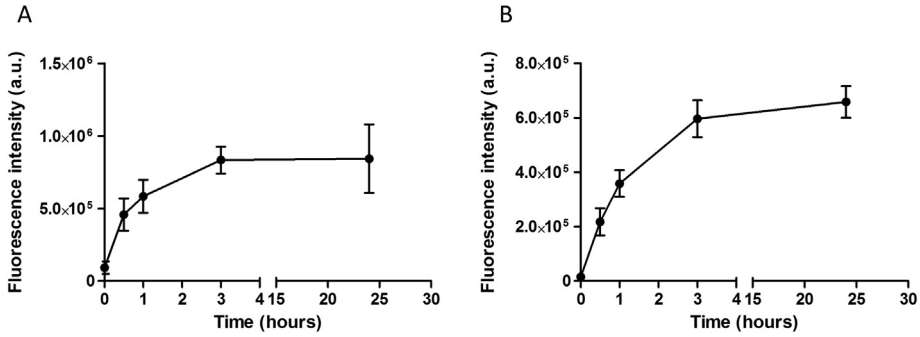


**Fig. 2.** Flow cytometry analysis of NPL endocytosis. 16HBE cells were treated for different times (0, 0.5, 1, 3 and 24 h) with NPL-FITC (A) or NPL-DiD (B). Results are expressed as mean ± SD of three independent experiments.

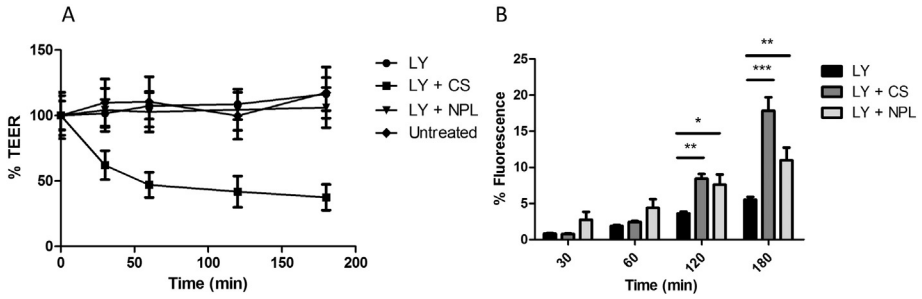


**Fig. 3.** A: Evaluation of tight junction opening, of 16HBE cells treated with either chitosan (CS) or NPL. Untreated cells were compared with cells treated with NPL, CS or lucifer yellow (LY). B: Evaluation of paracellular and transcellular permeability of LY. Cells monolayer with LY alone and in presence of CS or NPL. Results are expressed as the means ± SD of triplicate measurements of two independent experiments. *:$p < 0.05$; **:$p < 0.01$; ***:$p < 0.001$.

mice received 20 μl of PBS. The sacrifice was performed by cervical dislocation at different time points (1 and 3 h). The nasal cavities were then isolated and fixed in 4% paraformaldehyde (VWR International, France) for 24 h. Afterwards the nasal cavities were decalcified for 7 days in 10% EDTA (Sigma-Aldrich, France) and frozen in Tissue-Tek® OCT compound (Sakura® Finetek, USA), after which 10 μm slices were obtained. The nuclei were stained with Hoechst 33342 (ThermoFisher Scientific, France). Then slices were mounted with Dako fluorescence mounting medium (Agilent Technologies, France) and imaged with a confocal microscope (LSM 710, Zeiss, France).

### 2.12. Statistical analysis

One-way ANOVA and Two-way ANOVA plus post-test were used to determine the significance of variations between groups using GraphPad® Prism software.

## 3. Results

### 3.1. Characterization of NPL

$NP^+$ were made of porous cationic nanoparticles and lipids inserted into $NP^+$ to produce NPL (Fig. 1). The mean diameters of $NP^+$ and NPL were 70 and 76 nm and their polydispersity indexes were 0.23 and 0.21, respectively (Table 1). They were both highly cationic as their zeta potentials were +45.9 and +44.2 mV, respectively. Since the association of lipids with the $NP^+$ did not significantly modify their size and zeta potential, we concluded that these lipids were inserted into the core of the nanoparticles.

### 3.2. NPL endocytosis

We evaluated NPL endocytosis by airway epithelial cells using flow cytometry. The polysaccharidic part of the NPL was covalently labeled with FITC (NPL-FITC) while the lipidic core was labeled with the lipidic dye DiD (NPL-DiD). Following either the polysaccharidic or the lipidic part, the NPL endocytosis into epithelial cells increases in a similar way, reaching a plateau after 3 h (Fig. 2A and B). The endocytosis rate of NPL remained constant after 24 h. Moreover the kinetics profiles of endocytosis of the polysaccharidic or the lipidic parts of NPL showed the same trend for 24 h.

### 3.3. Evaluation of NPL transcytosis through the airway epithelial barrier

The 16HBE cells were cultured on Transwell® filters until the cells reached confluence (TEER value in the range of 250–750 $\Omega \times cm^2$). No decrease of TEER was observed after treatment with NPL indicating an absence of toxicity for these carriers. Chitosan (CS), that reportedly opens the TJ by an integrin mediated mechanism [37,38], was used as positive control (Fig. 3A).

To assess the permeability of the epithelial barrier, the transport of lucifer yellow (LY) across the airway mucosa was evaluated (Fig. 3). The paracellular permeation of LY reached 6% of the starting fluorescence after 3 h. A significantly higher permeation of LY (17.8% of initial fluorescence after 3 h) was observed when the tight junctions were opened using CS. The NPL induced a more rapid permeation of LY across the epithelial barrier (11% of initial fluorescence), but to a lesser extent than CS after 3 h.

Prior to the NPL transcytosis test, we first verified that NPL were able to cross the Transwell® filter (results not shown).

NPL-FITC or NPL-DiD were tested on the Transwell® model of the airway epithelial barrier in presence or absence of CS in order to evaluate NPL transcytosis. After 3 h incubation with NPL-FITC no significant transcytosis occurred. In addition, no fluorescence was detected in the basal compartment of the Transwell® treated with NPL-DiD (Fig. 4B). This confirmed that the NPL (both the polysaccharide and lipid parts) did not cross the epithelial barrier. Furthermore, even in conditions were tight junctions were opened, NPL transport was not increased (Fig. 4A and B).

### 3.4. Characterization of the OVA:NPL formulations

Different OVA:NPL formulations were prepared at different OVA:NPL (w/w) ratios.

Size analysis of the 1:0.5 OVA:NPL formulation by dynamic light scattering showed an aggregated formulation with a particle size of

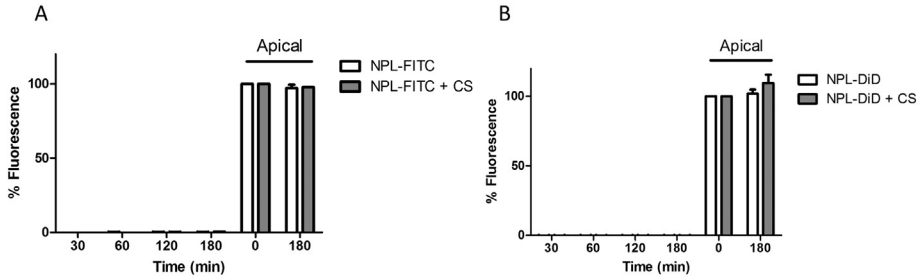


**Fig. 4.** Investigation of the *in vitro* translocation of NPL polysaccharide (A) and lipid part (B) across confluent 16HBE monolayers.

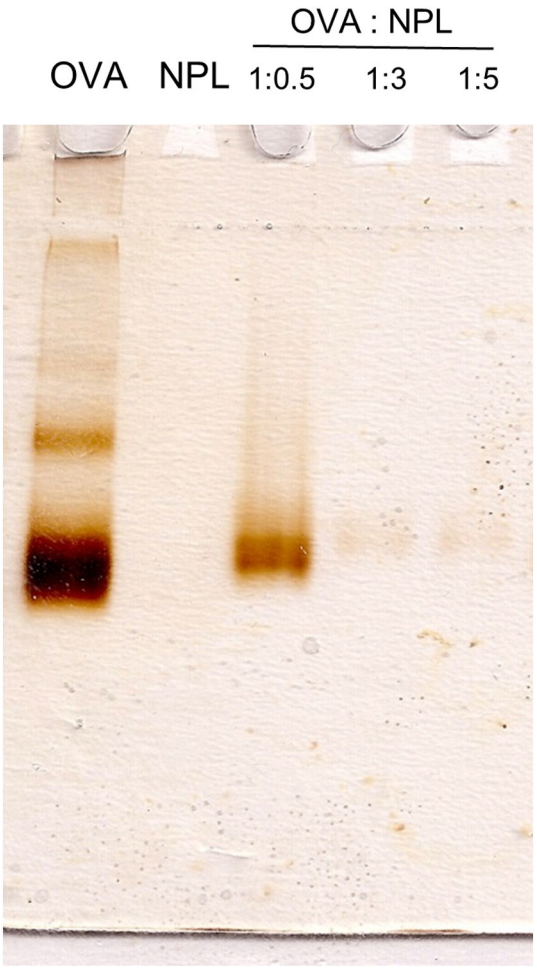


**Fig. 5.** Characterization of the ovalbumin (OVA) association to the NPL by native polyacrylamide gel (PAGE) electrophoresis using OVA:NPL at 1:0.5, 1:3 and 1:5 (w:w) ratios. Unbound proteins were revealed by silver nitrate staining.

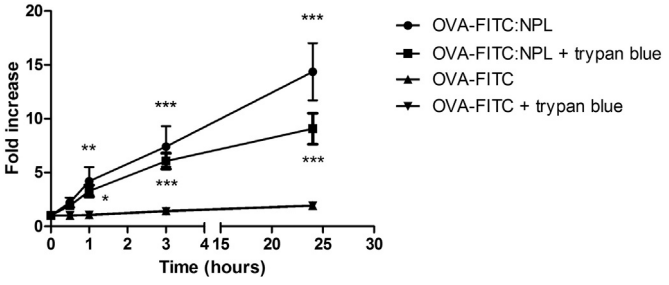


**Fig. 6.** Analysis of protein delivery by NPL into airway epithelial cells (16HBE) by flow cytometry. 16HBE were treated with free or formulated OVA-FITC for different time. Trypan blue was used to determine the % of protein bound on cell surface. Results are the mean of three independent experiments. *:$p < 0.05$; **:$p < 0.01$; ***:$p < 0.001$.

2.7 μm and a high polydispersity index (Table 1). Moreover, compared to the NPL alone (+44.2 mV), a decreased zeta potential was observed for this formulation (from +44 mV to +25 mV). The OVA association to the NPL was assessed by polyacrylamide gel-electrophoresis (PAGE) in non-denaturing conditions revealing the presence of unbound proteins (Fig. 5).

Increasing the protein:NPL mass ratio to 1:3, we observed that the size and zeta potential of OVA:NPL was unchanged relatively to NPL alone (Table 1). Native-PAGE electrophoresis (Fig. 5) revealed that the formulation of OVA:NPL at mass ratios of 1:3 and 1:5 led to the complete association of the ovalbumin to the NPL. The 1:3 formulation fits the optimal criteria for the study of protein delivery (similar size and zeta potential than NPL alone, complete protein association) and was used in the following experiments.

### 3.5. Kinetics of protein delivery into airway epithelial cells by NPL

The OVA delivery by NPL into airway epithelial cells was evaluated by flow cytometry. The epithelial cells were treated for different times (0.5, 1, 3 and 24 h) with OVA-FITC either free or formulated in the NPL at a 1:3 mass ratio. Trypan blue was used to quench the extracellular fluorescence adsorbed on cell surface [39].

Compared to $T_0$, a very low endocytosis was observed for OVA-FITC after 24 h (Fig. 6). Interestingly NPL highly increased OVA association with the cells (14.4 fold increase). Trypan blue experiment confirmed that OVA-FITC was endocytosed and that NPL highly increased its uptake.

### 3.6. In vitro transcytosis of free OVA or OVA:NPL

The transcytosis of free OVA or OVA:NPL was tested in the Transwell® model of the airway epithelial barrier, in the presence or absence of chitosan (CS). Neither free OVA nor OVA:NPL modified the TEER% in the absence of CS (Fig. 7A), while in the presence of CS the TEER% decreased to 45%, indicating the TJ opening.

The fluorescence of OVA-TRITC in the basal compartment of the Transwell® model was measured (Fig. 7B): after 3 h incubation, only 0.4% of the starting fluorescence of the OVA-TRITC was detected. No significant differences were observed in terms of OVA transcytosis between formulations even in the presence of CS. We concluded that NPL did not promote OVA transcytosis and that tight junction aperture by CS treatment was insufficient for the protein to cross the epithelial barrier.

### 3.7. In vivo biodistribution of OVA and OVA:NPL after nasal administration

We evaluated the *in vivo* biodistribution of free OVA *versus* NPL-loaded OVA for 2 days in mice using real time fluorescence optical imaging. Mice were nasally administered with free OVA-CF750® or OVA-CF750®:NPL; dorsal and ventral views of living animals were taken at defined time points (Fig. 8). As can be observed ventrally, a low fluorescence persistence of the unformulated protein is observed in the nose and totally disappeared after 1.5 h. Similar considerations

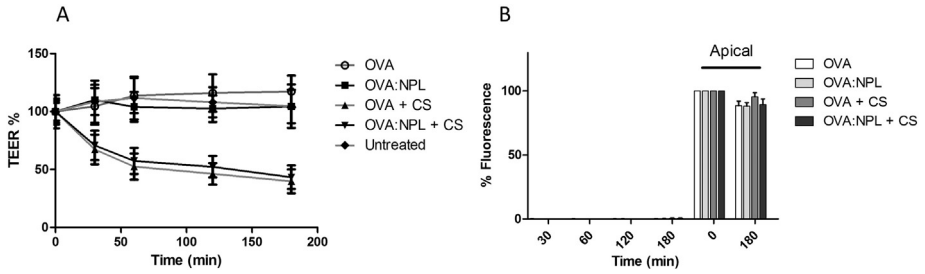


**Fig. 7.** *In vitro* passage of ovalbumin (OVA) free or formulated in NPL on 16HBE Transwell® model. Evaluation of the tight junction opening (A) and of the protein passage across the epithelial barrier (B).

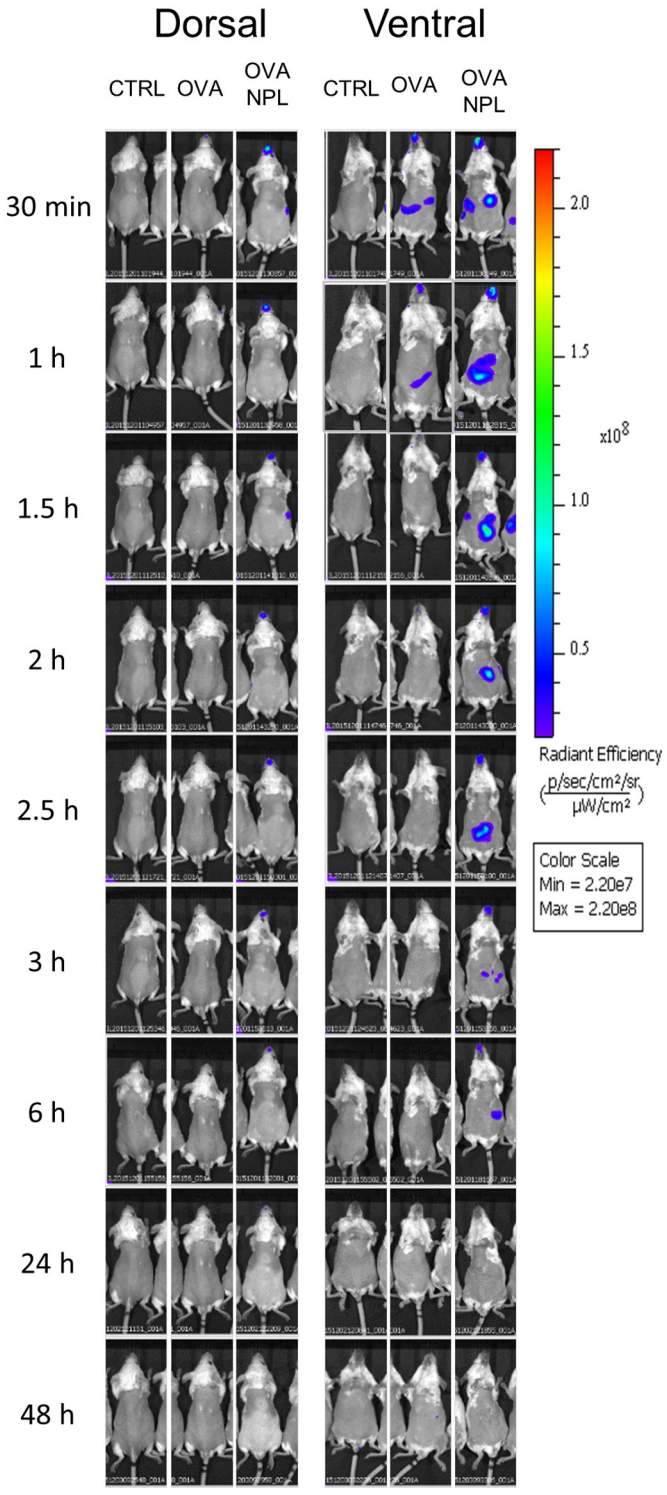


**Fig. 8.** Representative *in vivo* fluorescence images of OVA-CF750 biodistribution in mice. Mice were pre-treated with PBS (CTRL) or OVA-CF750, free and formulated in NPL. The ventral and the dorsal side of mice were imaged at different time points with *In Vivo* Imaging System IVIS® Spectrum ($n = 3$ per group).

have been brought dorsally. Moreover in the dorsal view we did not evidence fluorescence diffusion in the brain. Interestingly, NPL increased OVA residence time in the nose to at least 6 h (against 1.5 h for free OVA). Furthermore fluorescence related to labeled OVA was found in the feces (results not shown), suggesting its elimination.

### *3.8. Evaluation of NPL and OVA residence in the nose*

Consistent with the *in vivo* distribution results of OVA showing a discriminative time point of 1.5 h, we wanted to determine the localization of NPL and OVA in airway mucosa 1 h and 3 h after administration.

Mice were nasally instilled with OVA-TRITC:NPL-FITC and nose tissue, sampled at three different depths (I, II and III; Fig. 9), was subsequently analyzed after nuclei staining. We observed the presence of NPL after 1 h, but only at the mucosal level. Additionally, after confocal analysis, NPL endocytosis in airway mucosa was observable 1 h after administration and became more pronounced after 3 h. The NPL were observed in all the different depths of the nasal tissue, and also at the surface of the nose-associated lymphoid tissue (NALT) at 1 and 3 h after the nasal instillation. However, no NPL was detectable on the basal side of the epithelium, underlining the inability of NPL to cross this cellular barrier *in vivo*. Contrary to what is observed in whole nose biodistribution studies (Fig. 8), OVA was not detectable in these sections (Fig. 9).

## 4. Discussion

The nasal route of administration has been investigated in recent years as an effective mucosal site suitable for non-invasive vaccine delivery, and able to induce both systemic and mucosal immunity. Many studies have shown that nasal administration of particulate antigens (Ag) is more immunogenic compared with soluble ones [8]. For instance, it has been demonstrated that administering the whole, inactivated influenza virus was more immunogenic than administration of split, subunit or virosome vaccines [5]. We obtained similar results more than a decade ago when we demonstrated that maltodextrin nanoparticles, covered by a lipid bi-layer and loaded with HBs Ag and beta-galactosidase, were able to induce strong mucosal as well as systemic antibody and cytotoxic T cell responses, while free Ag was poorly immunogenic [40]. Recently, we demonstrated that nanoparticles loaded with *Toxoplasma gondii* Ag after intranasal administration were able to induce strong TH1 and TH17 responses, and were able to protect mice against an orally administered lethal challenge with wild parasite [33]. Furthermore, we also demonstrated that these nanoparticles were highly endocytosed *via* the clathrin pathway and highly exocytosed *via* a cholesterol-dependent pathway, delivering Ag within the cytosol of airway epithelial cells [34,41]. These results might explain the increased immunogenicity observed [33].

In this study, we further investigated the role of these supramolecular nanoparticles, made of a polysaccharide matrix loaded with phospholipids in their core (NPL), as potential vaccine delivery systems in airway mucosa, and the different constituents of these NPL (Fig. 1) were tracked to assess their fate after endocytosis in the mucosa.

We first confirmed that the lipid loading into the $NP^{+}$ did not vary the characteristics of size and zeta potential of the particles, suggesting the complete lipid incorporation into the maltodextrin structure (Table 1). As reported by Kroubi et al., the matrix saturation occurs at 70% of lipid loading (w/w); at higher percentages of lipid, irreversible aggregation of NPL was noted [42].

Due to the supramolecular structure of these nanoparticles made of polysaccharide and lipids we decided to follow the endocytosis of all their components in the cells in an effort to better define their role in protein delivery.

Interestingly, we observed similar uptake kinetics for both NPL components: polysaccharide and lipid (Fig. 2). This result suggests that the lipids are not released from the nanoparticles in the cells during their endocytosis. This is in contrast to liposomal preparations whose phospholipids were found to be converted to cellular phospholipid after lysosomal degradation [43], while our results indicate a high stability of the lipid (DPPG) inside the NPL.

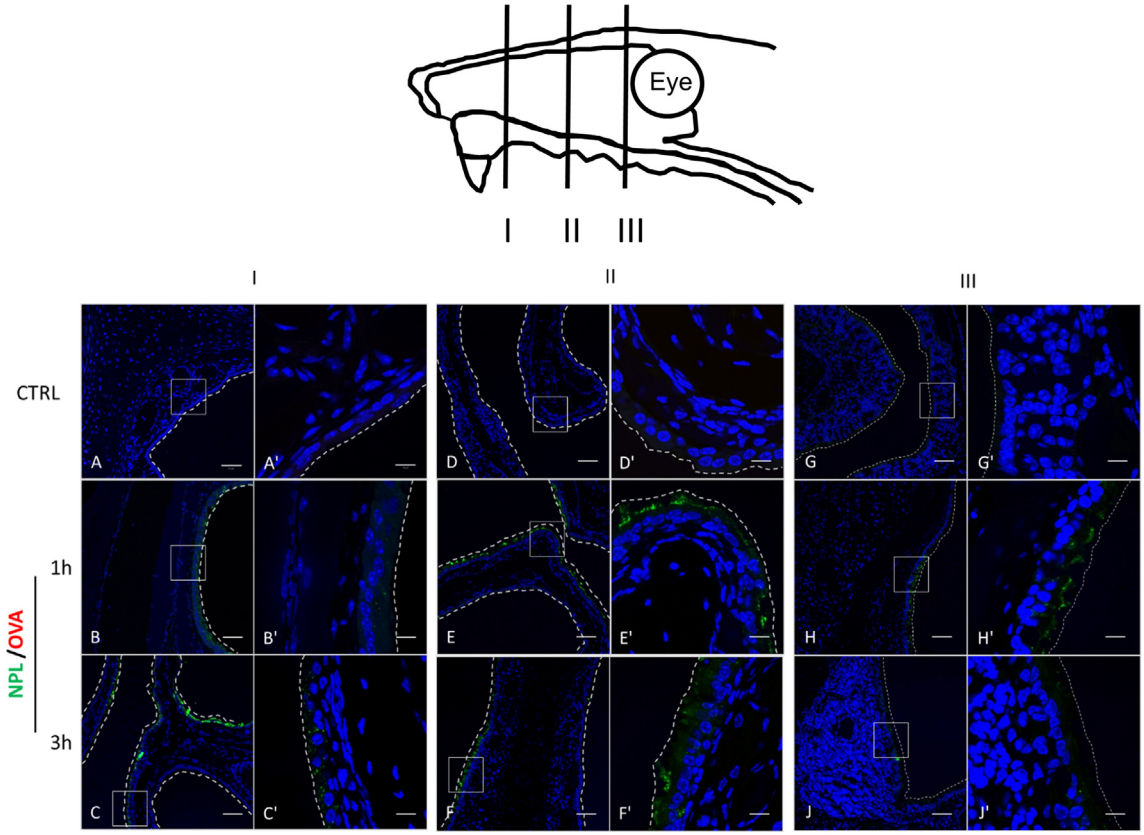


**Fig. 9.** Confocal microscopy analysis of frozen section of nasal mice tissue after different time points. Nasal biodistribution of the OVA-TRITC:NPL-FITC in three representative depth of the mice nose are reported, from the anterior segment (I) to the posterior segment (III). Enlargements of the regions in the white frames are reported. Nuclei were stained with Hoechst, NPL are labeled with FITC and OVA with TRITC. Scale bars 50 μm (A–J) and 10 μm (A′–J′). *In vivo* NPL endocytosis was confirmed and no NPL transcytosis was observed.

We thought it is essential to track the fate of these nanoparticles after nasal administration to fully understand how they deliver antigens in mucosa and potentially cross the mucosal barriers, both to learn their mechanism of action and investigate potential toxicity issues. We observed that NPL do not open the TJ and do not cross the airway epithelial barrier *in vitro* or *in vivo* (Figs. 4 and 9). Interestingly, in contrast to what is described for other particles [44], we were able to discount any nose-to-brain delivery of these nanoparticles as they were found not to cross the epithelial cells *in vitro* or *in vivo*. Nose-brain passage of nanoparticles and their potential toxicity would prevent further studies for vaccine applications [45].

However, in some circumstances, the epithelial barrier could become damaged leading to TJ opening [46,47]. Chitosan, a cationic polysaccharide polymer, opens TJ *in vitro* and *in vivo*, thus enhancing the passage of drugs unable to traverse the epithelial barrier by transcytosis by instead favoring paracellular passage [48]. We demonstrated that when the TJ were opened by the action of CS (Figs. 4 and 7), neither OVA (MW = 43.000 Da) nor NPL crossed the cells monolayer suggesting that opening the TJ aperture facilitates paracellular passage only for low molecular weight drugs. Furthermore cytotoxicity and genotoxicity studies were also performed on these cells and it was shown that even at high doses these NPL were not toxic [49].

The NPL can be loaded with a large amount of different proteins and the formulation is effective to induce humoral, cellular and mucosal responses when administered *via* the nasal route [33]. However, the underlying mechanisms of antigen delivery or antigen translocation by the NPL are not fully understood. Ovalbumin is a well-known vaccine model antigen, currently used as a template for nanoparticulate vaccines [3,50]. The formulated protein is efficiently delivered into airway epithelial cells (Fig. 6). Notably, we found that the formulation of OVA in NPL increased the protein delivery into cells 14 fold. We then studied the protein fate and its possibility to traverse the airway epithelial barrier. *In vitro* we did not observe any transcytosis of the free or formulated OVA (Fig. 7). We thus concluded that protein (in this case ovalbumin) is not transported across the epithelial barrier by transcytosis and that NPL do not facilitate nor induce this mechanism.

To study the permeability of the *in vitro* epithelial barrier model, since NPL and OVA cannot cross it, we used lucifer yellow as a low molecular weight molecule. Lucifer yellow crossed the epithelial barrier *in vitro*, without modifying the TEER%, *via* paracellular transport and pinocytosis allowing potential transcytosis [35,36,51], and its passage was increased by the TJ opening (Fig. 3). Its transfer across the epithelium was also enhanced by the NPL. We suggest that this increase could be directly linked to the increased intracellular traffic due to NPL endocytosis in a non-specific manner (Fig. 3) as no interaction between LY and NPL was observed (data not shown).

Finally, *in vivo* studies were necessary to understand the real fate of the NPL and the encapsulated protein within nasal mucosa.

Biodistribution studies performed by *in vivo* imaging allowed us to follow the protein distribution. We observed that after 1.5 h the protein administered alone had totally disappeared from the nasal area (Fig. 8), while nanoparticle formulated protein was still present after 6 h. This result suggests that NPL stay in the nose and potentially protect protein from degradation as had already been observed *in vitro* [34]. At this stage we considered two complementary possibilities emanating from this result: either the longer residence time of NPL/protein was due to adsorption at the surface of the mucosa, or OVA delivery within cells was more efficient when formulated in NPL. Confocal microscopy studies clearly showed that NPL were found in mucosa cells of the nose (Fig. 9). Interestingly, we still observed after 3 h the NPL in airway mucosa cells and no NPL was observed in the tissues underneath confirming the *in vitro* results. Free OVA, due to its fast degradation,

was observed only in minute amounts and poorly detectable on the nose tissue slices.

## 5. Conclusion

We studied the dynamics of nanoparticle and protein interaction with the nasal mucosa. Taken together, our results provide a framework of the whole mechanism for the bio-distribution of nanoparticle protein formulations. After nasal administration the NPL are endocytosed by airway epithelial cells and deliver the protein into the cells. We suggest that the *in vivo* increased residence time of OVA in airway cells might be due to an increased cellular protein uptake from OVA:NPL compared to free OVA, due at least in part to the partial protection of the protein from degradation afforded by its encapsulation within the NPL. The NPL are probably subsequently exocytosed and, following the mucociliary movement, are endocytosed by other/deeper cells in the nasal epithelium. During these processes, the NPL continue to deliver part of the encapsulated protein but do not cross the epithelial barrier. Contrary to what has been observed with other nanoparticles, NPL did not cross the mucosal barrier. Considering the previously demonstrated ability of NPL formulations to stimulate the immune system, and our findings that they do not cross airway epithelial barriers, these carriers are thus extremely interesting candidates for nasal vaccine delivery.

## Acknowledgments

The research leading to these results has received funding from the People Programme (Marie Curie Actions) of the European Union Seventh Framework Programme FP7/2007-2013/ under REA grant agreement no. [607690]. The authors would like to thank Michael Howsam for critically reading the manuscript. We also thank Olivier Briand from the University of Lille 2—INSERM U1011, Laura Choteau, Madjid Djouina and Audrey Langlois from the University of Lille 2 for their help in histology and technical support. The authors would like to thank the DigestScience Foundation for support.

## References

[1] V.B. Joshi, S.M. Geary, A.K. Salem, Biodegradable particles as vaccine antigen delivery systems for stimulating cellular immune responses, Hum. Vaccin. Immunotherapeutics 9 (2013) 2584–2590.
[2] P. Sahdev, L.J. Ochyl, J.J. Moon, Biomaterials for nanoparticle vaccine delivery systems, Pharm. Res. 31 (2014) 2563–2582.
[3] L. Zhao, A. Seth, N. Wibowo, C.X. Zhao, N. Mitter, C. Yu, A.P. Middelberg, Nanoparticle vaccines, Vaccine 32 (2014) 327–337.
[4] N.M. Molino, A.K. Anderson, E.L. Nelson, S.W. Wang, Biomimetic protein nanoparticles facilitate enhanced dendritic cell activation and cross-presentation, ACS Nano 7 (2013) 9743–9752.
[5] N. Hagenaars, E. Mastrobattista, H. Glansbeek, J. Heldens, H. van den Bosch, V. Schijns, D. Betbeder, H. Vromans, W. Jiskoot, Head-to-head comparison of four nonadjuvanted inactivated cell culture-derived influenza vaccines: effect of composition, spatial organization and immunization route on the immunogenicity in a murine challenge model, Vaccine 26 (2008) 6555–6563.
[6] J.M. Patel, V.F. Vartabedian, M.C. Kim, S. He, S.M. Kang, P. Selvaraj, Influenza virus-like particles engineered by protein transfer with tumor-associated antigens induces protective antitumor immunity, Biotechnol. Bioeng. 112 (2015) 1102–1110.
[7] Y. Vanloubbeeck, S. Pichyangkul, B. Bayat, K. Yongvanitchit, J.W. Bennett, J. Sattabongkot, K. Schaecher, C.F. Ockenhouse, J. Cohen, A. Yadava, P.v.v.s. group, Comparison of the immune responses induced by soluble and particulate *Plasmodium vivax* circumsporozoite vaccine candidates formulated in AS01 in rhesus macaques, Vaccine 31 (2013) 6216–6224.
[8] N. Lycke, Recent progress in mucosal vaccine development: potential and limitations, Nat. Rev. Immunol. 12 (2012) 592–605.
[9] A.S. Cordeiro, M.J. Alonso, M. de la Fuente, Nanoengineering of vaccines using natural polysaccharides, Biotechnol. Adv. 33 (2015) 1279–1293.
[10] Q. Liu, X. Zheng, C. Zhang, X. Shao, X. Zhang, Q. Zhang, X. Jiang, Conjugating influenza a (H1N1) antigen to n-trimethylaminoethylmethacrylate chitosan nanoparticles improves the immunogenicity of the antigen after nasal administration, J. Med. Virol. 87 (2015) 1807–1815.
[11] R. Pabst, Mucosal vaccination by the intranasal route. Nose-associated lymphoid tissue (NALT)—structure, function and species differences, Vaccine 33 (2015) 4406–4413.
[12] A. Beloqui, M.A. Solinis, A.R. Gascon, A. del Pozo-Rodriguez, A. des Rieux, V. Preat, Mechanism of transport of saquinavir-loaded nanostructured lipid carriers across the intestinal barrier, J. Control. Release 166 (2013) 115–123.
[13] M. Gidwani, A.V. Singh, Nanoparticle enabled drug delivery across the blood brain barrier: in vivo and in vitro models, opportunities and challenges, Curr. Pharm. Biotechnol. 14 (2014) 1201–1212.
[14] D. Guarnieri, A. Falanga, O. Muscetti, R. Tarallo, S. Fusco, M. Galdiero, S. Galdiero, P.A. Netti, Shuttle-mediated nanoparticle delivery to the blood-brain barrier, Small 9 (2013) 853–862.
[15] L. Han, Y. Zhao, L. Yin, R. Li, Y. Liang, H. Huang, S. Pan, C. Wu, M. Feng, Insulin-loaded pH-sensitive hyaluronic acid nanoparticles enhance transcellular delivery, AAPS PharmSciTech 13 (2012) 836–845.
[16] C. Schimpel, B. Teubl, M. Absenger, C. Meindl, E. Frohlich, G. Leitinger, A. Zimmer, E. Roblegg, Development of an advanced intestinal in vitro triple culture permeability model to study transport of nanoparticles, Mol. Pharm. 11 (2014) 808–818.
[17] B. Bharatwaj, R. Dimovski, D.S. Conti, S.R. da Rocha, Polymeric nanocarriers for transport modulation across the pulmonary epithelium: dendrimers, polymeric nanoparticles, and their nanoblends, AAPS J. 16 (2014) 522–538.
[18] R. Fowler, D. Vllasaliu, F.H. Falcone, M. Garnett, B. Smith, H. Horsley, C. Alexander, S. Stolnik, Uptake and transport of B12-conjugated nanoparticles in airway epithelium, J. Control. Release 172 (2013) 374–381.
[19] B. Rothen-Rutishauser, C. Muhlfeld, F. Blank, C. Musso, P. Gehr, Translocation of particles and inflammatory responses after exposure to fine particles and nanoparticles in an epithelial airway model, Part. Fibre Toxicol. 4 (2007) 9.
[20] E. Brun, F. Barreau, G. Veronesi, B. Fayard, S. Sorieul, C. Chaneac, C. Carapito, T. Rabilloud, A. Mabondzo, N. Herlin-Boime, M. Carriere, Titanium dioxide nanoparticle impact and translocation through ex vivo, in vivo and in vitro gut epithelia, Part. Fibre Toxicol. 11 (2014) 13.
[21] D. Cremaschi, C. Porta, R. Ghirardelli, Different kinds of polypeptides and polypeptide-coated nanoparticles are accepted by the selective transcytosis shown in the rabbit nasal mucosa, Biochim. Biophys. Acta 1416 (1999) 31–38.
[22] N. Hagenaars, M. Mania, P. de Jong, I. Que, R. Nieuwland, B. Slutter, H. Glansbeek, J. Heldens, H. van den Bosch, C. Lowik, E. Kaijzel, E. Mastrobattista, W. Jiskoot, Role of trimethylated chitosan (TMC) in nasal residence time, local distribution and toxicity of an intranasal influenza vaccine, J. Control. Release 144 (2010) 17–24.
[23] X. Han, N. Corson, P. Wade-Mercer, R. Gelein, J. Jiang, M. Sahu, P. Biswas, J.N. Finkelstein, A. Elder, G. Oberdorster, Assessing the relevance of in vitro studies in nanotoxicology by examining correlations between in vitro and in vivo data, Toxicology 297 (2012) 1–9.
[24] R. Rosenthal, M.S. Heydt, M. Amasheh, C. Stein, M. Fromm, S. Amasheh, Analysis of absorption enhancers in epithelial cell models, Ann. N. Y. Acad. Sci. 1258 (2012) 86–92.
[25] X. Cao, H. Lin, L. Muskhelishvili, J. Latendresse, P. Richter, R.H. Heflich, Tight junction disruption by cadmium in an in vitro human airway tissue model, Respir. Res. 16 (2015) 30.
[26] D. Patel, S. Naik, K. Chuttani, R. Mathur, A.K. Mishra, A. Misra, Intranasal delivery of cyclobenzaprine hydrochloride-loaded thiolated chitosan nanoparticles for pain relief, J. Drug Target. 21 (2013) 759–769.
[27] S. Jesus, E. Soares, J. Costa, G. Borchard, O. Borges, Immune response elicited by an intranasally delivered HBsAg low-dose adsorbed to poly-epsilon-caprolactone based nanoparticles, Int. J. Pharm. (2016).
[28] B. Forbes, C. Ehrhardt, Human respiratory epithelial cell culture for drug delivery applications, Eur. J. Pharm. Biopharm. 60 (2005) 193–205.
[29] Y. Grumbach, N.V. Quynh, R. Chiron, V. Urbach, LXA4 stimulates ZO-1 expression and transepithelial electrical resistance in human airway epithelial (16HBE14o-) cells, Am. J. Phys. Lung Cell. Mol. Phys. 296 (2009) L101–L108.
[30] H. Wan, H.L. Winton, C. Soeller, G.A. Stewart, P.J. Thompson, D.C. Gruenert, M.B. Cannell, D.R. Garrod, C. Robinson, Tight junction properties of the immortalized human bronchial epithelial cell lines Calu-3 and 16HBE14o, Eur. Respir. J. 15 (2000) 1058–1068.
[31] B. Forbes, A. Shah, G.P. Martin, A.B. Lansley, The human bronchial epithelial cell line 16HBE14o—as a model system of the airways for studying drug transport, Int. J. Pharm. 257 (2003) 161–167.
[32] A. Paillard, C. Passirani, P. Saulnier, M. Kroubi, E. Garcion, J.P. Benoit, D. Betbeder, Positively-charged, porous, polysaccharide nanoparticles loaded with anionic molecules behave as 'stealth' cationic nanocarriers, Pharm. Res. 27 (2010) 126–133.
[33] I. Dimier-Poisson, R. Carpentier, T.T. N'Guyen, F. Dahmani, C. Ducournau, D. Betbeder, Porous nanoparticles as delivery system of complex antigens for an effective vaccine against acute and chronic *Toxoplasma gondii* infection, Biomaterials 50 (2015) 164–175.
[34] C. Dombu, R. Carpentier, D. Betbeder, Influence of surface charge and inner composition of nanoparticles on intracellular delivery of proteins in airway epithelial cells, Biomaterials 33 (2012) 9117–9126.
[35] I. George, S. Vranic, S. Boland, A. Courtois, A. Baeza-Squiban, Development of an in vitro model of human bronchial epithelial barrier to study nanoparticle translocation, Toxicol. in Vitro 29 (2015) 51–58.
[36] M.S. Goligorsky, K.A. Hruska, Transcytosis in cultured proximal tubular cells, J. Membr. Biol. 93 (1986) 237–247.
[37] L.W. Hsu, Y.C. Ho, E.Y. Chuang, C.T. Chen, J.H. Juang, F.Y. Su, S.M. Hwang, H.W. Sung, Effects of pH on molecular mechanisms of chitosan-integrin interactions and resulting tight-junction disruptions, Biomaterials 34 (2013) 784–793.
[38] L.W. Hsu, P.L. Lee, C.T. Chen, F.L. Mi, J.H. Juang, S.M. Hwang, Y.C. Ho, H.W. Sung, Elucidating the signaling mechanism of an epithelial tight-junction opening induced by chitosan, Biomaterials 33 (2012) 6254–6263.
[39] J. Nuutila, E.M. Lilius, Flow cytometric quantitative determination of ingestion by phagocytes needs the distinguishing of overlapping populations of binding and ingesting cells, Cytometry A 65 (2005) 93–102.

[40] A. Debin, R. Kravtzoff, J.V. Santiago, L. Cazales, S. Sperandio, K. Melber, Z. Janowicz, D. Betbeder, M. Moynier, Intranasal immunization with recombinant antigens associated with new cationic particles induces strong mucosal as well as systemic antibody and CTL responses, Vaccine 20 (2002) 2752–2763.
[41] C.Y. Dombu, M. Kroubi, R. Zibouche, R. Matran, D. Betbeder, Characterization of endocytosis and exocytosis of cationic nanoparticles in airway epithelium cells, Nanotechnology 21 (2010) 355102.
[42] M. Kroubi, S. Daulouede, H. Karembe, Y. Jallouli, M. Howsam, D. Mossalayi, P. Vincendeau, D. Betbeder, Development of a nanoparticulate formulation of diminazene to treat African trypanosomiasis, Nanotechnology 21 (2010) 505102.
[43] J. Dijkstra, M. van Galen, D. Regts, G. Scherphof, Uptake and processing of liposomal phospholipids by Kupffer cells in vitro, Eur. J. Biochem./FEBS 148 (1985) 391–397.
[44] Z. Liu, M. Jiang, T. Kang, D. Miao, G. Gu, Q. Song, L. Yao, Q. Hu, Y. Tu, Z. Pang, H. Chen, X. Jiang, X. Gao, J. Chen, Lactoferrin-modified PEG-co-PCL nanoparticles for enhanced brain delivery of NAP peptide following intranasal administration, Biomaterials 34 (2013) 3870–3881.
[45] A. Elder, R. Gelein, V. Silva, T. Feikert, L. Opanashuk, J. Carter, R. Potter, A. Maynard, Y. Ito, J. Finkelstein, G. Oberdorster, Translocation of inhaled ultrafine manganese oxide particles to the central nervous system, Environ. Health Perspect. 114 (2006) 1172–1178.
[46] S. Ganesan, A.T. Comstock, U.S. Sajjan, Barrier function of airway tract epithelium, Tissue Barriers 1 (2013), e24997.
[47] I. George, G. Naudin, S. Boland, S. Mornet, V. Contremoulins, K. Beugnon, L. Martinon, O. Lambert, A. Baeza-Squiban, Metallic oxide nanoparticle translocation across the human bronchial epithelial barrier, Nanoscale 7 (2015) 4529–4544.
[48] K. Sonaje, E.Y. Chuang, K.J. Lin, T.C. Yen, F.Y. Su, M.T. Tseng, H.W. Sung, Opening of epithelial tight junctions and enhancement of paracellular permeation by chitosan: microscopic, ultrastructural, and computed-tomographic observations, Mol. Pharm. 9 (2012) 1271–1279.
[49] M. Merhi, C.Y. Dombu, A. Brient, J. Chang, A. Platel, F. Le Curieux, D. Marzin, F. Nesslany, D. Betbeder, Study of serum interaction with a cationic nanoparticle: implications for in vitro endocytosis, cytotoxicity and genotoxicity, Int. J. Pharm. 423 (2012) 37–44.
[50] S.L. Demento, W. Cui, J.M. Criscione, E. Stern, J. Tulipan, S.M. Kaech, T.M. Fahmy, Role of sustained antigen release from nanoparticle vaccines in shaping the T cell memory phenotype, Biomaterials 33 (2012) 4957–4964.
[51] D. Tyteca, P. Van Der Smissen, F. Van Bambeke, K. Leys, P.M. Tulkens, P.J. Courtoy, M.P. Mingeot-Leclercq, Azithromycin, a lysosomotropic antibiotic, impairs fluid-phase pinocytosis in cultured fibroblasts, Eur. J. Cell Biol. 80 (2001) 466–478.